Available online at www.sciencedirect.com
SCIENCE DIRECT®
Journal of Solid State Chemistry 178 (2005) 2998–3003
JOURNAL OF SOLID STATE CHEMISTRY
www.elsevier.com/locate/jssc

Electrochemical zinc insertion into $W_{18}O_{49}$: Synthesis and characterization of new bronzes

A. Martínez-de la Cruz[a], U. Amador[b], J. Rodríguez-Carvajal[c], F. García-Alvarado[b,*]

[a]*Instituto de Ingeniería Civil, Facultad de Ingeniería Civil, Universidad Autónoma de Nuevo León, Apartado Postal 17, San Nicolás de los Garza, N.L. Mexico*
[b]*Departamento de Química, Universidad San Pablo-CEU, Urb. Montepríncipe, 28668 Boadilla del Monte, Madrid, Spain*
[c]*Laboratoire Léon Brillouin (CEA-CNRS), Centre d'Etudes de Saclay, 91191 Gif-sur-Yvette Cedex, France*

Received 14 April 2005; received in revised form 13 July 2005; accepted 13 July 2005
Available online 18 August 2005

Abstract

Divalent zinc ions have been electrochemically inserted into $W_{18}O_{49}$, producing zinc bronzes. Under our experimental conditions, $W_{18}O_{49}$ accepts zinc reversibly as a guest up to 0.9 ions per formula. The reaction seems to proceed through the formation of a solid solution in which the W–O framework of the parent oxide is maintained. The location of the Zn^{2+} ions in the framework of $W_{18}O_{49}$ has been determined by neutron diffraction on a chemically prepared sample having the composition $Zn_{0.34}W_{18}O_{49}$. As a main result, we found that Zn prefers to insert in one of the four types of quadrangular tunnels. More precisely, it is displaced from the center to occupy a low coordination site. This result indicates that a significant covalent character exists in the Zn–O bond.

Keywords: Electrochemical insertion; Zinc insertion; Zinc tungsten bronzes; Structure determination; Neutron diffraction

1. Introduction

Tungsten bronzes A_xWO_3 have been widely studied since the first member of this class of compounds was reported by Whöler in 1823 [1]. The large number of compounds that can be included in this category are mainly described by different arrangements of [W–O_6] octahedra [2,3]. Open structures can be built up using corner shared [W–O_6] octahedra and have shown the capability of hosting metallic ions of different size. Besides alkali and alkaline earth metals [3–6], some transition metals and most rare earth metals [7,8] can occupy the tunnels of W–O open frameworks. The wide range of non-stoichiometry, as well as the appearance of very interesting electrical and optical properties [9,10], make research on preparation of new tungsten bronzes interesting.

Although other transition metal oxides, as for instance MoO_3 and V_2O_5, are able to form bronzes A_xMoO_3 and $A_xV_2O_5$, the largest family is the so-called tungsten bronzes and a great variety of them are well known, especially those obtained by alkali metal insertion (A_xWO_3 with A = Li, Na and K) [11].

In a previous work we have reported the formation of novel zinc tungsten bronzes by electrochemical zinc insertion into the monoclinic form of WO_3 [12]. The monoclinic form is the most widely studied among the polymorphs of WO_3. Nevertheless, the hexagonal form, first prepared by Gérand et al. [13], presents the most open structure and is very attractive for insertion reactions.

Another tungsten oxide with some structural features similar to those of h–WO_3 is $W_{18}O_{49}$, which we have used as a host for zinc insertion. This oxide has proved to be a good host for monovalent ions like lithium and sodium [14,15], but also for divalent ions. We prepared bronzes $Mg_xW_{18}O_{49}$ by chemical methods [16], but

*Corresponding author. Fax: +34 91 351 04 96.
E-mail address: flaga@ceu.es (F. García-Alvarado).

0022-4596/$ - see front matter © 2005 Elsevier Inc. All rights reserved.
doi:10.1016/j.jssc.2005.07.008

failed to study the electrochemical behavior by means of two electrode cells $Mg\|W_{18}O_{49}$. We have now chosen a more suitable divalent cation to study the relationships between size, charge and extent of intercalation reaction. Although rechargeable batteries made using $W_{18}O_{49}$ as the positive electrode are not realistic, the results obtained from our previous reports on Li, Na and Mg intercalation, and the present may be extrapolated to lighter and suitable electrodes.

2. Experimental

The reduced tungsten oxide $W_{18}O_{49}$ was prepared by high-temperature reaction between metallic W and fresh WO_3, mixed in the appropriate ratio. Reagents were placed in a quartz ampoule under vacuum, and then annealed at 1000 °C for 3 days. Fresh WO_3 was obtained by thermal decomposition of H_2WO_4 at 850 °C for 3 days. The as-prepared microcrystals of $W_{18}O_{49}$ exhibit a rectangular platelet shape (typically ca. 1.5–3 μm long and 0.25–0.50 μm wide).

For the electrochemical characterization, a mixture of the parent oxide with carbon black and ethylene propylene diene terpolymer were prepared (ratio of components 89:10:1 by weight). The mixture, pressed into pellets, was used as the positive electrode of electrochemical cells with the following configuration:

$$Zn/0.2\,mol\,dm^{-3}(CF_3SO_3)_2Zn \text{ in PC} + DMSO(1:4)/W_{18}O_{49} \text{ mixture},$$

where PC is propylene carbonate and DMSO is dimethyl sulfoxide. All the electrochemical experiments were made under potentiostatic conditions using two electrode cells. Metallic zinc was used as both counter and reference electrode. Low voltage scan rates were used (+10 mV/2, 24 or 32 h) in order to get closer to thermodynamic equilibrium conditions. In some cases, cells were stopped at different stages of discharge and the positive electrode material analyzed by X-ray diffraction and electron diffraction.

For neutron diffraction experiments on $Zn_xW_{18}O_{49}$, electrochemically synthesized material was not used due to the large amount of sample needed. Instead, a chemical route at room temperature was followed. A bronze $Zn_xW_{18}O_{49}$ was synthesized by direct reaction of $W_{18}O_{49}$ with a 1 mol dm^{-3} solution of diethyl zinc in hexane. In order to achieve a high content of inserted ion, an oxide to Zn ratio of 1:2 was used. The mixture was stirred for 7 days and afterwards filtrated. The powder obtained was washed several times with dry hexane. The ratio of metals was analyzed by means of Energy Dispersive Spectroscopy using a JEOL 2000FX transmission electron microscope.

A preliminary characterization of the parent and the electrochemically inserted products was performed by X-ray powder diffraction (XRD) on a Philips X'Pert diffractometer equipped with $Cu(K_{\alpha1+\alpha2})$ radiation ($\lambda = 1.5418$ Å) and a nickel filter.

The XRD pattern used for structure determination of $Zn_xW_{18}O_{49}$ was obtained on a Bruker D8 diffractometer of Bragg–Bentano geometry, equipped with a primary graphite monochromator giving a monochromatic beam of $Cu(K_{\alpha1})$ radiation ($\lambda = 1.5406$ Å). This pattern was recorded at room temperature, working in transmission mode using glass capillaries of 0.5 mm diameter filled with the samples, to overcome a severe preferred orientation effect. To minimize the absorption of heavy atoms such as tungsten, the sample was mixed with powdered diamond in a weight ratio 1:1. The measured angular range (from $2\theta = 5^\circ$ to 60°), the step size (0.02) and counting times were selected to ensure sufficient resolution and statistics. A sample from the same batch was also studied at room temperature by neutron diffraction (NPD) on the diffractometer G4.2 of the Orphée Reactor at Laboratoire Léon Brillouin. A monochromatic beam of wavelength 2.3433 Å was selected with a Ge(004) monochromator; for this radiation the instrumental resolution is within the range $2.7 \times 10^{-3} \leqslant (\Delta Q/Q) \leqslant 0.022$.

The structure was refined by the Rietveld method using the FULLPROF program [17]; both the XRD and NPD data were simultaneously fitted, the fitting process considered finished when convergence was reached. The models proposed for $W_{18}O_{49}$ by Viswanathan et al. [18] and Lamire et al. [19], were used as structure starting models although the choice was not found to be crucial. Zinc ions were located within the structure by Fourier synthesis.

3. Results and discussion

3.1. Zinc insertion in $W_{18}O_{49}$

Fig. 1a shows the voltage-composition plot obtained in the first discharge–charge cycle of a cell, bearing $W_{18}O_{49}$ as the active material of the positive electrode, under potentiostatic conditions (10 mV/2 h). It can be seen that the quantity of Zn^{2+} inserted when a cell is discharged up to 0.01 V vs. Zn^{2+}/Zn^0, corresponds to ~0.9 Zn/formula. Insertion of Zn into $W_{18}O_{49}$ is reversible as can also be seen in the same figure. The charge proceeds following a parallel curve until the upper cut-off voltage is reached. At this stage not all the Zn ions have been extracted. Approximately 20% of inserted Zn ions are trapped. This is the usual observation for electrodes fabricated by pressing powdery components and is due to grains that became electrically disconnected after the discharge process.

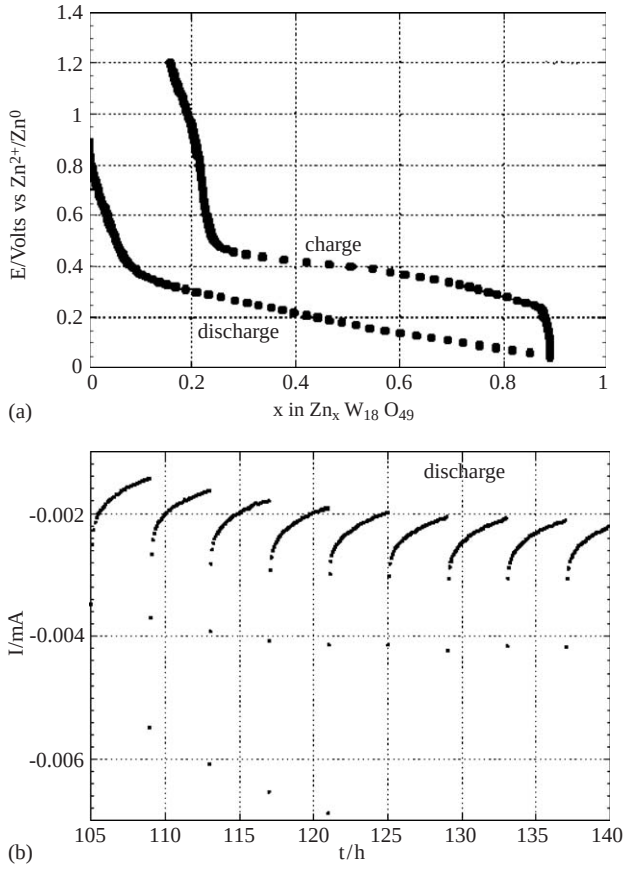

Fig. 1. (a) Voltage-composition plot obtained from potentiostatic cycling of a cell Zn//$W_{18}O_{49}$. (b) Relaxation of current in the composition range $Zn_{0.18}W_{18}O_{49}$–$Zn_{0.43}W_{18}O_{49}$.

The zinc content obtained at 0.01 V is not the maximum quantity that $W_{18}O_{49}$ may accept. Note from Fig. 1a that the discharge–charge cycle is affected by a high polarization (ca. 200 mV). Although the contribution of the electronic conductivity of the electrode to polarization was reduced in other electrochemical runs by mixing the oxide with larger quantities of carbon black, similar results were obtained when zinc insertion proceeded. This seems to indicate that polarization is mainly associated with the slow kinetics of diffusion process.

The reaction may be highly affected by the mobility of the ion through the framework. Size is not the key factor in the Zn case, since despite the similarity of size between lithium and zinc ions ($r^{VI}_{Li^+} = 0.76$ Å, $r^{VI}_{Zn^{2+}} = 0.74$ Å) [20,21], the general behavior regarding insertion reactions is quite different. When compared with lithium, the double positive charge of zinc cation rules the extent of the insertion reaction. Although the results obtained for zinc have not been obtained under total equilibrium, the difference is clear: 0.9 Zn^{2+} per formula with respect to ca. 23 Li^+ per formula [14]. It is interesting to note the case of the magnesium ion [16]. The divalent ion Mg^{2+} has both ionic radii ($r^{VI}_{Mg^{2+}} = 0.72$ Å) and charge similar to those of Zn^{2+}. Therefore, the quantity that can be inserted, 0.9 ion/formula [16], is similar to the quantity found for the Zn^{2+} case. Thus, if ionic potential (Ze/r^2) was chosen as the ruling factor, Li^+, with a value of 1.73, should behave differently from Mg^{2+} and Zn^{2+}, whose values (3.85 and 3.65), respectively are more similar but greater than in the case of Li^+. For cations with high ionic potential, the high covalent character of the guest–host interaction is expected to affect diffusion and hence insertion extent.

On the other hand Na^+ is a large cation ($r^{VI}_{Na^+} = 0.72$ Å) [21] that can be inserted into the same host. Although the value of ionic potential is 0.96, the extent of the reaction (ca. 2 Na^+/formula [15]) is not larger than in the case of Li^+. Therefore, it seems that in the case of Na the insertion extent is not limited by diffusion but by the sites available for Na^+.

It should be noted that when either lithium or sodium ions are electrochemically inserted in $W_{18}O_{49}$, equilibrium conditions are easy to achieve [12,15] even for the voltage scan rate used in the experiment shown in Fig. 1 (10 mV/2 h). However, during the electrochemical insertion of zinc, we observed that increasing time at every voltage step, i.e to 10 mV/24 h, did not result in any relevant decreasing polarization. Since a very slow diffusion of the divalent ion is expected when compared with monovalent ions, a slower cycling rate had to be used to get close to equilibrium. At 10 mV/32 h, a complete discharge–charge cycle would have taken 8 months, and although such experiments were started, we did not get any reliable data because a longer time period favors the corrosion of metallic zinc. Hence, reliable data regarding content of Zn are those obtained for voltage scanning rates as the one corresponding to data of Fig. 1. For all experiments carried out we have detected a slow relaxation of current after every voltage step indicating the slow kinetics of the reaction (see Fig. 1b). For high Zn contents current does not reach zero after voltage steps but interesting information can be extracted. Every relaxation curve have the same shape and no anomalies can be observed indicating that the system is crossing a solid solution region [22]. Nevertheless, since the electrochemical reaction is likely far from equlibrium, the true nature of the region may be still uncertain. However, additional information has been obtained by means of structural characterization.

Both X-ray and electron diffraction data of electrochemically obtained samples $Zn_xW_{18}O_{49}$ indicated that the W–O framework is maintained, as expected for relatively small quantities of inserted ion into an open structure. Regarding the sites that zinc may occupy when inserted in $W_{18}O_{49}$, we again deal with the differences between ions of similar size but different charge. It is known that a very large number of lithium

ions (up to 23 Li/$W_{18}O_{49}$) can be accommodated into the structure of $W_{18}O_{49}$ [14]; thus, most likely every type of tunnel, hexagonal, quadrangular and triangular, is occupied. Now, we find that only ca. 0.9 Zn can be hosted by this material. Note that magnesium, which has the same charge and similar radius, can be inserted in $W_{18}O_{49}$ up to a similar quantity ($Mg_{0.9}W_{18}O_{49}$ [16]). We have found the same situation when Mg^{2+} or Zn^{2+} is inserted in h–WO_3 (h–$Mg_{0.15}WO_3$ [16] and h–$Zn_{0.13}WO_3$ [23]).

To obtain a precise structural model of the bronze, both neutron and X-ray diffraction experiments were carried out. For this purpose we prepared a sample following the chemical route described in the experimental section and analyzed the ratio of metals by EDS. As a product of the direct reaction between $W_{18}O_{49}$ and diethyl zinc in hexane, a sample with a composition $Zn_{0.34(6)}W_{18}O_{49}$ was obtained.

Accordingly with the interpretation of electrochemical data shown in Fig. 1, one phase may be present in our sample although the alternative explanation assuming a biphasic region could not be fully discarded. However, neither the XRD data nor the neutron diffraction pattern (NPD) suggest the existence of two different phases (see Fig. 2) supporting the first interpretation. Besides, the experiments carried out by electron diffraction did not show anything different from the parent cell. The same result was obtained by electron diffraction for different $Zn_xW_{18}O_{49}$ ($0 \leqslant x \leqslant 0.9$) obtained electrochemically.

The fitting of XRD and NPD data was accomplished using as a starting model only one phase with the W–O framework of $W_{18}O_{49}$; the zinc ions were located by Fourier synthesis. Significant occupation was found only at (~0.6 0 ~0.6). The final structural parameters are collected in Table 1, whereas Table 2 shows selected zinc-oxygen inter-atomic distances. Calculated composition corresponds to $Zn_{0.36}W_{18}O_{49}$ in agreement with the result obtained by EDS analysis ($Zn_{0.34(6)}W_{18}O_{49}$). In Fig. 3a, a schematic representation of the structure is depicted; Fig. 3b shows the first co-ordination sphere of zinc ions. As stated above, the W–O framework is retained in the inserted material, the distances and angles (not shown) essentially the same as in the parent compound. Zinc ions are located in one of the four different quadrangular tunnels existing in the structure, those centered at (0.4286 1/2 0.3418). However, zinc ions are displaced from the center towards the oxygen atoms to occupy a more suitable position, allocating themselves at distances close to the average one observed in many zinc oxides ($d(Zn^{2+}–O^{2-}) \approx 2.14$ Å, $r^{VI}(Zn^{2+}) = 0.74$ Å, $r^{VI}(O^{2-}) = 1.40$ Å) [20]. Thus, if the co-ordination sphere of Zn^{2+} is limited to this distance, an unusual 3-fold co-ordination is obtained including one very short Zn–O distance (2.07 Å). However, considering larger distances, up to 2.6 Å, an octahedral environment is completed,

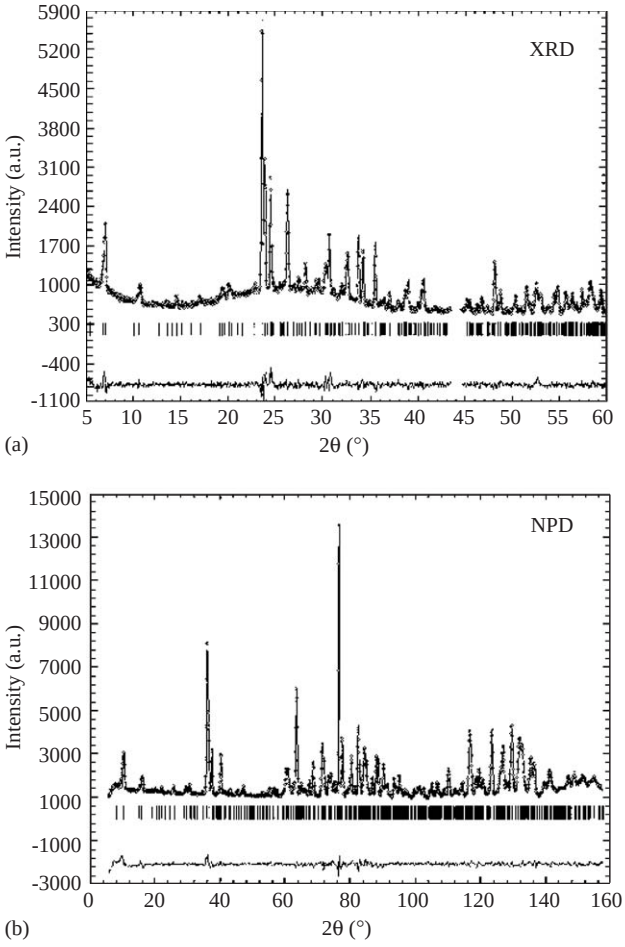

Fig. 2. Graphic result of the fitting of the X-ray (a) and neutron (b) powder diffraction data of $Zn_xW_{18}O_{49}$ (x~0.36 at RT): experimental (points), calculated (solid line) and difference (bottom). In the XRD pattern, the excluded region (43.5–44.5°) corresponds to the strong (111) peak of diamond used to minimize absorption.

though it is very distorted (see Fig. 3b and Table 2) with average Zn–O distance of 2.31 Å. The fact that zinc ions are located in positions where it is co-ordinated to six oxygen atoms, some of them at somewhat short distances ($\leqslant 2.14$ Å), suggests that the inserted zinc ions are strongly bonded to some of the oxygen of the framework. This seems to be an indication of a significant covalent character in the Zn–O bond and it may be the origin of the slow kinetics of the insertion reaction.

Note that structure determination showed only one position for Zn. Then $Zn_{\sim 0.36}W_{18}O_{49}$ can be thought of as a $W_{18}O_{49}$ framework and some Zn^{2+} ions randomly distributed among the (~0.6 0 ~0.6) and equivalent positions.

4. Conclusions

Electrochemical insertion of Zn into $W_{18}O_{49}$ has shown that new Zn-bronzes can be obtained. Under our

Table 1
Final structural parameters of $Zn_{0.36(4)}W_{18}O_{49}$

Atom	x/a	y/b	z/c	Atom	x/a	y/b	z/c
Zn[a]	0.594(5)	0	0.613(6)				
W(1)[b]	0.0726(9)	1/2	0.006(2)	O(9)	0.450(1)	0	0.167(1)
W(2)	0.092(1)	1/2	0.288(1)	O(10)	0.021(1)	1/2	0.713(1)
W(3)	0.127(1)	1/2	0.757(1)	O(11)	0.042(1)	1/2	0.126(2)
W(4)	0.221(1)	1/2	0.574(1)	O(12)	0.134(1)	1/2	0.910(2)
W(5)	0.259(1)	1/2	0.015(1)	O(13)	0.139(1)	1/2	0.433(2)
W(6)	0.276(1)	1/2	0.254(1)	O(14)	0.141(1)	1/2	0.635(2)
W(7)	0.353(1)	1/2	0.858(1)	O(15)	0.201(1)	1/2	0.102(1)
W(8)	0.414(1)	1/2	0.539(1)	O(16)	0.190(1)	1/2	0.281(2)
W(9)	0.452(1)	1/2	0.169(1)	O(17)	0.238(1)	1/2	0.856(2)
O(1)[c]	0.080(1)	0	0.005(1)	O(18)	0.309(1)	1/2	0.725(2)
O(2)	0.081(1)	0	0.283(1)	O(19)	0.314(1)	1/2	0.541(1)
O(3)	0.130(1)	0	0.765(1)	O(20)	0.3424(9)	1/2	0.165(1)
O(4)	0.217(1)	0	0.577(1)	O(21)	0.350(1)	1/2	0.383(2)
O(5)	0.247(1)	0	0.002(2)	O(22)	0.366(1)	1/2	0.014(2)
O(6)	0.2767(9)	0	0.245(2)	O(23)	0.464(1)	1/2	0.878(2)
O(7)	0.3618(9)	0	0.880(1)	O(24)	0.522(1)	1/2	0.319(2)
O(8)	0.420(1)	0	0.542(1)	O(25)	1/2	1/2	1/2

S.G. $P2/m$ (num. 10), $a = 18.2961(6)$ Å, $b = 3.7769(1)$ Å, $c = 14.0107(4)$ Å, $\beta = 115.191(2)^\circ$, $V = 876.11(4)$ Å^3, $Z = 4$, $\rho = 8.66(1)$ g/cm^3, global $\chi^2 = 4.4$.
DRX pattern: $R_B = 0.090$, $R_{exp} = 0.126$, $R_{wp} = 0.169$, $\chi^2 = 1.79$.
Neutron pattern: $R_B = 0.048$, $R_{exp} = 0.041$, $R_{wp} = 0.109$, $\chi^2 = 6.98$.
[a]Occ(Zn) = 0.09(1) Composition: $Zn_{0.36(4)}W_{18}O_{49}$.
[b]B (Å^2)$_{Metals} = 0.27(8)$.
[c]B (Å^2)$_{Oxygen} = 0.22(5)$.

Table 2
Selected inter-atomic zinc-oxygen distances less than 2.8 Å in $Zn_{0.36(4)}W_{18}O_{49}$

Zn–O(6)	2.36(9)
Zn–O(8)	2.07(8)
Zn–O(21)	2.14(5) × 2
Zn–O(25)	2.59(5) × 2
Average	2.312(3)
Distortion: $1/n\Sigma[(d_i - <d>)/\langle d\rangle]^2$	85.19×10^{-4}

experimental conditions, bronze reaction is reversibly, reaching the maximum composition $Zn_{0.9}W_{18}O_{49}$. The W–O framework of the parent is maintained upon zinc insertion in as much as the reaction proceeds through the formation of the solid solution $Zn_xW_{18}O_{49}$ with $0 \leqslant x \leqslant 0.9$.

Structural determination carried out on a chemically prepared sample with composition $Zn_{0.34}W_{18}O_{49}$ indicates that Zn^{2+} is located in a highly distorted octahedron with three very short Zn–O distances ($\leqslant 2.14$ Å). This is an indication of a significant covalent character in the Zn–O bond. Hence, a relationship between this structural feature and the slow kinetics of reaction observed is likely to exist.

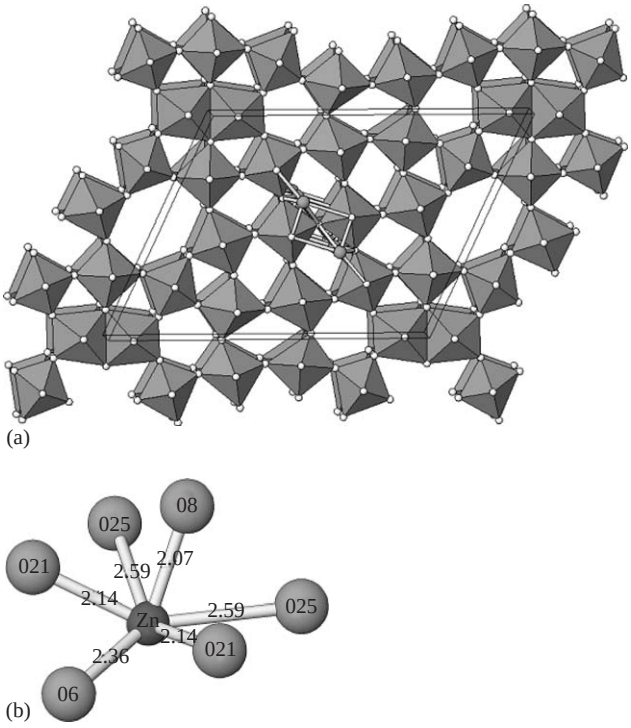

Fig. 3. Schematic representation of (a) the structure of $Zn_{0.36}W_{18}O_{49}$ projected along the b-axis and (b) coordination sphere of Zn ions.

Acknowledgments

We would like to thank the Ministerio de Educación y Ciencia for funding the project MAT2004-03070-C05-01. The access to the neutron facilities at the Laboratoire Léon Brillouin was supported by the ARI action of the HPRI Program of the European Community. AMC also thanks CONACYT for supporting the project 43800 and UANL for its invaluable support through the program PAICYT (2004).

References

[1] F. Whöler, Ann. Chim. Phys. 43 (1823) 29.
[2] P. Hagenmuller, Comprehensive Inorganic Chemistry, vol. 4, Oxford, 1973, p. 572.
[3] K.H. Cheng, M.S. Whittingham, Solid State Ion. 1 (1980) 151.
[4] B. Schlasche, R. Schöllhorn, Rev. Chem. Miner. 19 (1982) 534.
[5] R.C.T. Slade, B.C. West, G.P. Hall, Solid State Ion. 32–33 (1989) 154.
[6] C. Michel, M. Hervieu, R.J.D. Tilley, B. Raveau, J. Solid State Chem. 52 (1984) 281.
[7] I.J. McColm, R.J.D. Tilley, C.P.M. Barton, N.N. Greenwood, J. Solid State Chem. 16 (1976) 265.
[8] C. Grenthe, M. Sundberg, J. Solid State Chem. 167 (2002) 412.
[9] C.G. Granqvist, Sol. Energy Mater. Sol. Cells 60 (2000) 201.
[10] I. Chaitanya Lekshmi, A. Gayen, V. Prasad, S.V. Subramanyam, M.S. Hedge, Mater. Res. Bull. 37 (2002) 1815.

[11] K.H. Cheng, A.J. Jacobson, M.S. Whittingham, Solid State Ion. 5 (1981) 355.
[12] A. Martínez de la Cruz, L.M. Torres-Martínez, F. García-Alvarado, E. Morán, M.A. Alario-Franco, J. Mater. Chem. 8 (1998) 1805.
[13] B. Gérand, G. Nowogrocki, J. Guenot, M. Figlarz, J. Solid State Chem. 29 (1979) 429.
[14] A. Martínez-de la Cruz, F. García-Alvarado, E. Morán, M.A. Alario-Franco, L.M. Torres-Martínez, J. Mater. Chem. 5 (1995) 513.
[15] A. Martínez-de la Cruz, L.M. Torres-Martínez, F. García-Alvarado, E. Morán, M.A. Alario-Franco, J. Solid State Chem. 151 (2000) 220.
[16] A. Martínez-de la Cruz, L.M. Torres-Martínez, F. García-Alvarado, E. Morán, M.A. Alario-Franco, Solid State Ion. 84 (1996) 181.
[17] J. Rodriguez-Carvajal, Physica B 19 (1993) 55.
[18] K. Viswanathan, K. Brandt, E. Salje, J. Solid State Chem. 36 (1981) 45.
[19] M. Lamire, P. Labbe, M. Goreaud, B. Raveau, Rev. Chim. Miner. 24 (1987) 369.
[20] R.D. Shannon, C.T. Prewitt, Acta Crystallogr. B 25 (1969) 925.
[21] R.D. Shannon, Acta Crystallogr. A 32 (1976) 751.
[22] Y. Chabre, NATO ASI Ser. 305 (1993) 181.
[23] A. Martínez de la Cruz, Ph. D. Dissertation, Universidad Complutense, Madrid, Spain, 1997.